IEEE Open Journal of
Power Electronics

Received 23 November 2022; revised 18 January 2023; accepted 30 January 2023. Date of publication 2 February 2023;
date of current version 16 February 2023. The review of this article was arranged by Associate Editor Tommaso Caldognetto.

Digital Object Identifier 10.1109/OJPEL.2023.3241778

Efficiency Optimization via Mission Profile-Based Power Routing by Design of Hybrid Grid Connecting Converter Architecture

JOSCHA SCHAUMBURG, JOHANNES KUPRAT (Graduate Student Member, IEEE), MARIUS LANGWASSER (Member, IEEE), AND MARCO LISERRE (Fellow, IEEE)

Chair of Power Electronics, Kiel University, 24118 Kiel, Germany

CORRESPONDING AUTHOR: JOSCHA SCHAUMBURG (e-mail: js@tf.uni-kiel.de)

This work was supported by the German Federal Ministry of Education and Research (BMBF) within Kopernikus Project ENSURE "New ENergy Grid StructURes for the German Energiewende" under Grant 03SFK1I0-2.

ABSTRACT Hybrid grids with low voltage direct current (LVdc) distribution are an attractive opportunity for the integration of electric vehicle charging stations and photovoltaic power plants. With dc connectivity reduced power losses are possible, however, multiple conversion stages can impair an efficient operation. A solution can be the use of an "interconnected" architecture that allows the integration of multiple insulated dc and ac grids. The reconfiguration of this modular topology allows optimization for different design objectives. This work investigates the system efficiency-optimized reconfiguration. Two approaches for deriving the reconfiguration of the hybrid grid connecting converter architecture based on mission profiles are proposed. A validation of the analysis via laboratory results is given.

INDEX TERMS DC microgrid, efficiency optimization, hybrid grids, power routing.

I. INTRODUCTION

Renewable energy sources, battery energy-storage systems and the increasing number of electric vehicle charging stations can be integrated into the electric distribution grid with the use of dc networks efficiently [1], [2], [3]. For dc integration, topics like reactive power and grid frequency become obsolete and advantages as reduced power losses and system complexity arise [4]. Although research is done in the field of dc protection [5], [6], [7], the established protection schemes as well as the still present ac-loads like households and consumers make the use of hybrid distribution systems the preferable choice [8], [9], [10]. The transition from ac to hybrid grids has to be done with highest caution to transfer e.g. the dc grid's selling point of improved efficiency. For large hybrid networks, the increased power losses induced by multiple power conversion stages are a main challenge. Phase-Shedding can improve the system efficiency during operation [11], [12]. At the design stage, the efficiency can be improved on the component and the converter level, e.g. enabled by the usage of wide-bandgap semiconductors [13] and resonant converters [14]. With these approaches the losses of the single power conversion stages can be reduced, however, the potential on system level improvement is not exploited. The hybrid grid connecting converter architecture (Fig. 1) in the version of an interconnected topology (IT) can connect multiple insulated dc and ac grids. This dc-multibus structure can provide higher system efficiency through a reduced number of conversion stages [15]. The modular approach of the converter can improve resilience, increase fault tolerance, allow use of components with lower ratings and enable easier maintenance during operation. In [16], a mission profile-based design procedure is applied to this architecture - via reconfiguration of power electronic building blocks (PEBBs) - for converter downsizing and increased fault tolerance.

The main contributions of this paper are:

- mission profile-based design is applied to the hybrid grid connecting converter architecture to improve its efficiency.
- Two approaches are proposed to find the optimal configuration via passive power routing by reconfiguration.

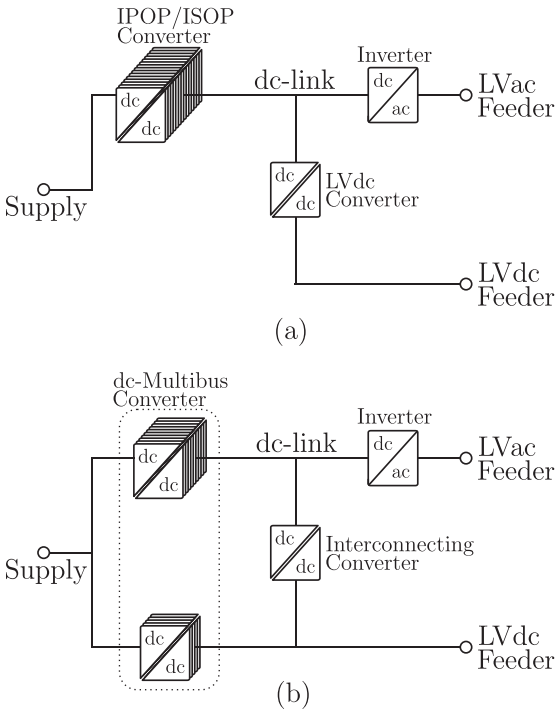

FIGURE 1. Hybrid grid connecting converter architectures: (a) Non-Interconnected Topology (NIT) and (b) Interconnected Topology (IT) with case study of $N_{MB} = 15$.

- Results of the approaches are compared and an approach with low modeling effort and sufficient accuracy is identified.
- The effectiveness of the reconfiguration on the efficiency is validated on a laboratory setup.

This article is structured as follows. In Section II, the investigated hybrid grid connecting converter architecture and a use case topology are introduced. Section III describes the mission profile-based efficiency optimization, divided into three subsections: firstly, the system efficiency is examined with special regard to the topology configuration. Secondly, the investigated LV grid mission profiles are shown. Lastly, two mission profile-based optimization approaches that allow an optimal topology configuration choice are highlighted. In Section IV, the results of the efficiency optimization analysis are shown. A laboratory validation is given in Section V, highlighting the system efficiency influence of the reconfiguration. Finally, the work is concluded in Section VI.

II. DESCRIPTION OF THE TOPOLOGY

More charging stations for electric vehicles, renewable energy sources and battery energy-storage systems can be integrated via a LVdc grid in the distribution grid efficiently. The connection of a supply grid with LV dc and ac grids at the load end can be enabled by the two hereafter introduced hybrid grid connecting converter architectures. A benchmark topology shown in Fig. 1(a) - which copes with grid insulation requirements by using an insulated dc/dc connection - is denoted as non-interconnected topology (NIT) [17], [18], [19]. An input-parallel-output-parallel (IPOP) or input-series-output-parallel (ISOP) isolated dc/dc converter - depending on the voltage of the supply grid - is used to provide insulation between the supply grid and the LV grids. A dual active bridge (DAB) is used to connect the LVdc grid to the dc-link in this topology, which is also connected to the LVac grid via a three-phase ac/dc converter. As a case study to connect to an ac supply grid, a cascaded H-bridge converter (CHB) is considered for the rectifier stage. By reconfiguring the converters of the NIT, without changing the individual converters themselves, the IT in Fig. 1(b) [19] can be obtained. Each full bridge cell and a corresponding DAB within the ISOP converter will be referred to as multibus (MB) PEBB with total number of N_{MB} cells. For the IT, a direct connection to the LVdc feeder is given by $N_{MB,LVdc}$ MB PEBBs. This reconfiguration is described by the link ratio

$$\xi = \frac{N_{MB,LVdc}}{N_{MB}} \quad . \tag{1}$$

A dc-multibus structure is created which allows direct power transfer between supply grid and LVdc feeder. The second bus is connected to the dc-link with $N_{MB,LVac}$ MB PEBBs. The converter replacing the LVdc DAB of the NIT and interconnecting the dc-link and the LVdc grid is hereafter referred to as interconnecting DAB. However, the rating of the converter is kept the same for both topologies, so that the potential of solely applying the reconfiguration can be evaluated. With the IT, multiple power paths can be included in a hybrid grids-feeding topology. The IT can have an enhanced system efficiency [19] and also gives the advantage of an additional design parameter - the link ratio ξ. Improvement of the fault tolerance by adding redundancy and the possibility of downsizing the interconnecting DAB are further benefits [16] as well as having higher efficiency by internal power routing. All these benefits can be realized without the need for an increased number of semiconductors.

III. MISSION PROFILE-BASED EFFICIENCY OPTIMIZATION

Next, the use of ITs link ratio ξ for system efficiency improvement is investigated. The concept of *Power Routing by Design* (PRD) is introduced - an approach to find an optimal link ratio ξ_{opt} based on mission profiles with given loading conditions.

The calculation method presented in [19] is applied to compute the system efficiency η_{sys}. High/medium-frequency transformer losses, switching losses, and conduction losses are considered - the analytic equations are based on ideal waveforms and depend on the loading conditions. An efficiency function depending on the converter output power P_{out} and the overall internal losses P_{loss} can be assigned to every converter

$$\eta(P_{out}) = \frac{P_{out}}{P_{in}} = \frac{P_{out}}{P_{loss}(P_{out}) + P_{out}} \quad . \tag{2}$$

For every operation point (P_{LVac} P_{LVdc}), the system efficiency is determined using these efficiency curves with a

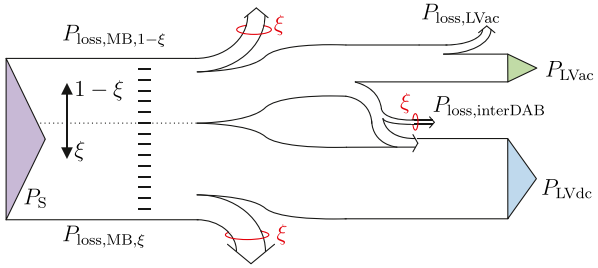

FIGURE 2. Power flow Sankey diagram of the IT for $P_{\text{LVdc}} > 0$, $P_{\text{LVac}} > 0$ (link ratio $\xi = \frac{9}{15}$). The influence of the link ratio ξ on the losses is highlighted.

non-conserved power flow calculation together with the information of the link ratio ξ [20].

A. LINK RATIO INFLUENCE ON THE SYSTEM EFFICIENCY

First, the link ratio influence on the system efficiency η_{sys} is investigated. The voltages considered in the theoretical analysis are 11 kV for the phase to phase RMS voltage of the MVac grid, 230 V phase to neutral RMS voltage for the LVac grid, 800 V for the dc-link, and 750 V for the LVdc grid. The same power is processed by each of the PEBBs, based on the connection of these PEBBs to the dc-link or to the LVdc grid the power which must be processed by the interconnecting DAB to satisfy the point of operation of the LV grids can be determined. The link ratio ξ boundaries are given by $0 \leq \xi \leq \frac{N_{\text{MB}}-1}{N_{\text{MB}}}$, which results in N_{MB} different possible configurations. Choosing $\xi = 0$ gives the NIT as benchmark. The configuration characterized by $\xi = 1$ is excluded as a special case where all PEBBs are connected to the LVdc grid.

In Fig. 2, a power flow diagram is given for an arbitrary operation point where both LV grids consume active power from the supply grid. The power distribution and the converter losses are influenced by the link ratio, which is highlighted by showing the internal power flow within the hybrid grid connecting converter architecture and the distribution of the different converter losses. This leads to an adapted system efficiency for every operation point. Fig. 3 shows the system efficiency for three different link ratios, herein and in the following 1 p.u. = 500 kW. The operation points which fulfill the condition

$$\frac{P_{\text{LVdc}}}{P_{\text{LVac}}} = \frac{N_{\text{MB,LVdc}}}{N_{\text{MB,LVac}}} = \frac{\xi}{1-\xi} \tag{3}$$

are especially highlighted. This constraint (3) gives an optimal system efficiency for quadrant 1 with $P_{\text{LVac}} > 0$ and $P_{\text{LVdc}} > 0$ as well as for quadrant 3 with reverse power flow feeding power to the supply grid. In this case, the interconnected DAB is unloaded - when neglecting the losses of the LVac converter. Hence, the ratio of LV powers at the respective operation point is the basis for the configuration of the PEBBs.

With the influence of the LVac converter, the corresponding elliptical shaped lines of equal efficiency and the local maximum are shifted to operation points with slightly higher values of P_{LVdc}. This local efficiency optimum is significantly influenced by the link ratio. Therefore, it is possible to chose an optimal link ratio for any operation point to unload the interconnecting DAB as far as possible for optimal system efficiency.

Looking at quadrant 2 with $P_{\text{LVac}} < 0$ and $P_{\text{LVdc}} > 0$ and vice versa in quadrant 4 high system efficiency is achieved with absolute power values almost equal $|P_{\text{LVac}}| \approx |P_{\text{LVdc}}|$. In this case, no power absorption from the supply grid is needed, because a direct power transfer via the interconnecting DAB is possible. Even higher efficiencies can be achieved for $|P_{\text{LVdc}}| \gg |P_{\text{LVac}}|$ and high values of the link ratio (e.g. Fig. 3(c)). With the non-linear behavior of the efficiency curves transferring power via the dc-multibus converter stage is more beneficial than transferring power via the three-phase converter and the interconnecting DAB.

For all operating points, the optimal link ratios ξ_{opt} in terms of system efficiency are shown in Fig. 4. Most suitable for quadrants 1 and 3 is a link ratio which fits the inherent load distribution of the LV grids, in this way the interconnecting DAB is unloaded by routing the power so that it is transferred directly to the sink. The operation points described by (3) are surrounded by different radiating triangular segments symmetrically. In Fig. 5, these results are highlighted for LV powers which satisfy the condition $P_{\text{LVac}} + P_{\text{LVdc}} = 1$ p.u.. For a given area of operation points a specific link ratio is optimal. The difference in the system efficiency maximum of the different curves parametrized by the link ratio stems from the LVac converter loss influence. The maximum efficiency in these two quadrants is achieved when the power is transferred directly where it is needed without using the interconnecting DAB as a bypass.

For quadrant 2 ($P_{\text{LVac}} < 0$ and $P_{\text{LVdc}} > 0$) and quadrant 4 (vice versa) the minimum link ratio ξ_{min} and maximum link ratio ξ_{max} are the best choices. For the case of $|P_{\text{LVdc}}| > |P_{\text{LVac}}|$ in these quadrants, the power difference between the LV grids is transferred between the supply grid and the LVdc grid. With the maximum link ratio this power transfer leads to the highest efficiency. Therefore, it is beneficial to connect as many PEBBs as possible directly to the LVdc grid. The NIT - which gives the minimum link ratio - leads to the highest efficiency for operation points in quadrants 2 and 4 with $|P_{\text{LVac}}| > |P_{\text{LVdc}}|$ and for very low $|P_{\text{LVdc}}|$ values in quadrants 1 and 3. In Fig. 6, the benefit of choosing the optimal link ratio is highlighted by the possible efficiency improvement. When using the optimal link ratio ξ_{opt} instead of the NIT (link ratio $\xi_{\text{NIT}} = 0$), the efficiency can be improved by up to 3.0 $\Delta\%$. Using the IT with a proper choice of reconfiguration is beneficial for most operation points, in all other cases - where the NIT is better - the NIT should be used.

B. MISSION PROFILES CONSIDERED FOR EFFICIENCY PERFORMANCE EVALUATION

The LV grids are described by mission profiles, shown in Fig. 7, which are used to carry out the subsequent analysis. The operating points are described by a set M of 2-tuples (P_{LVac} P_{LVdc}) which give the loading conditions. Linear

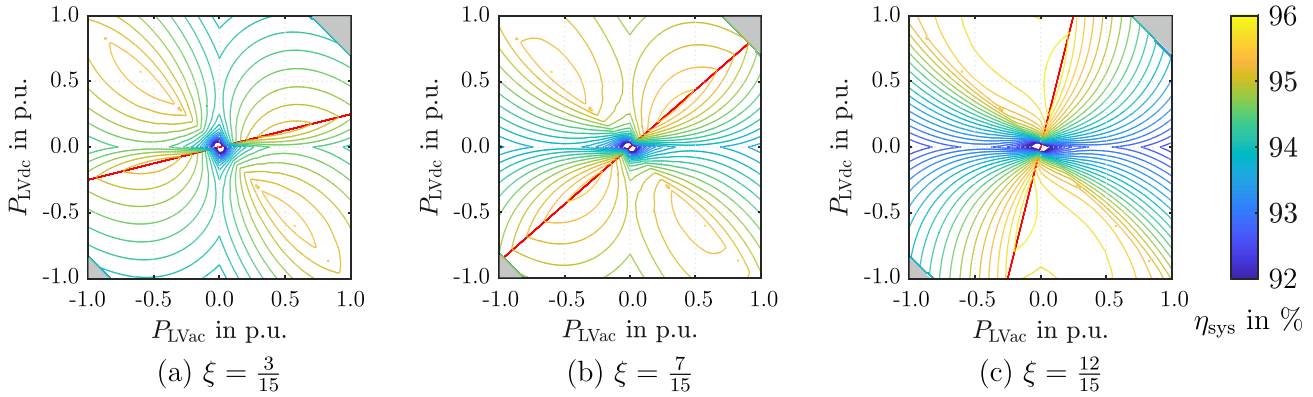

FIGURE 3. System efficiency η_{sys} for different configurations - (a) $\xi = \frac{3}{15}$, (b) $\xi = \frac{7}{15}$ and (c) $\xi = \frac{12}{15}$. MB PEBB limits are given as gray triangles, these operation points are excluded. Optimal link ratio shown with red lines.

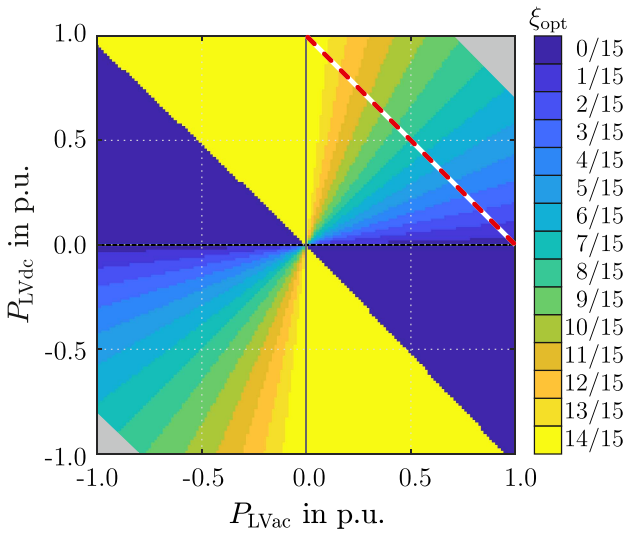

FIGURE 4. Optimal link ratio ξ_{opt} in terms of system efficiency and operation points with equal total cumulative output power $P_{LVac} + P_{LVdc} = 1$ p.u. highlighted with red dotted line.

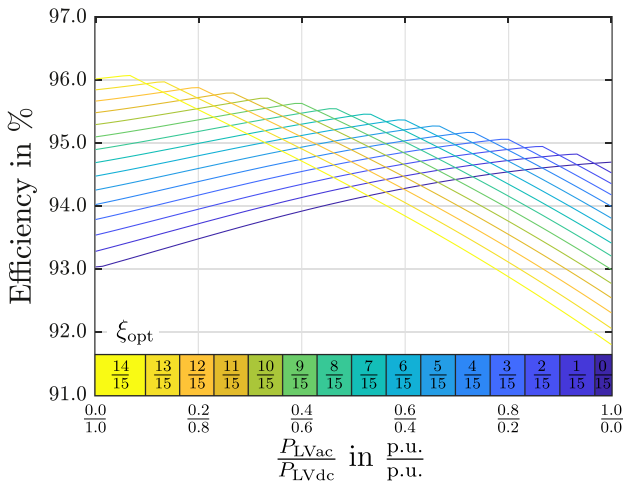

FIGURE 5. System efficiency η_{sys} for operation points highlighted with $P_{LVac} + P_{LVdc} = 1$ p.u.

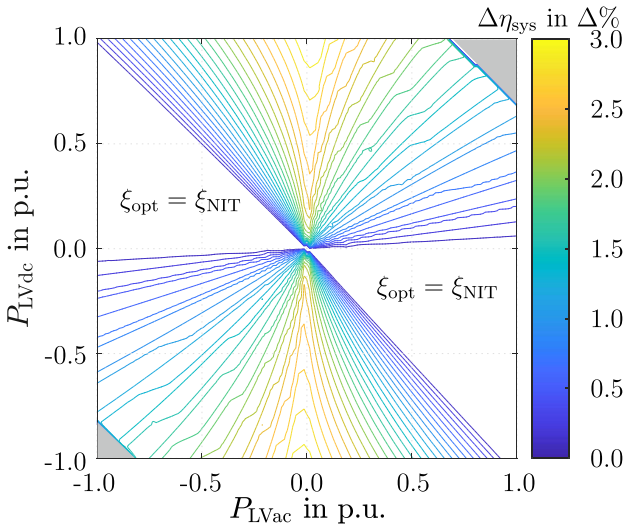

FIGURE 6. Eff. difference $\Delta\eta_{sys} = \eta_{sys,\xi_{opt}} - \eta_{sys,\xi_{NIT}}$.

superposition of a photovoltaic (PV) profile [21] and an average electric vehicle (EV) charging demand profile [22] is used for the LVdc profile use cases 1 and 2. Use case 3 for the LVdc profile considers a constant base load. Standard load profiles G0, G6 or H0 from the German Association of Energy and Water Industries (ger. BDEW) are used for the LVac profile. General commercial loads are represented by the G0 profile. The G6 profile gives a load profile for companies with high weekend consumption like restaurants and cinemas. Private household consumption is given by the H0 profile.

C. POWER ROUTING BY DESIGN

In the following, two approaches which give a proper link ratio ξ configuration are compared. Choosing an optimal design for maximum overall system efficiency under given loading conditions based on mission profiles is the goal of the approaches.

In the first approach, the system efficiency for every operation point of the mission profile trajectory is taken into

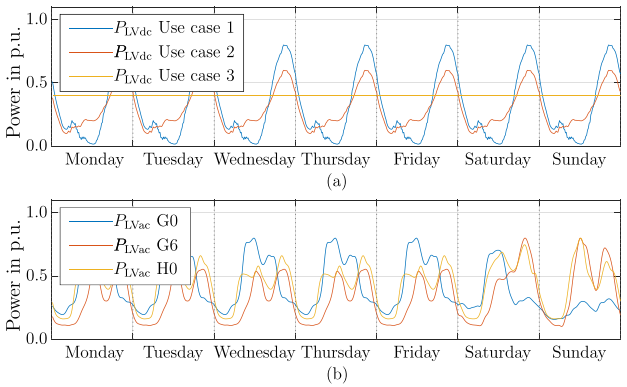

FIGURE 7. Mission profiles (normalized) for (a) the LVdc grid (use case 1 with high amount of EV and PV, use case 2 (low EV and PV) and use case 3 (constant power load)) and (b) the LVac grid (G0, G6 and H0 standard load profiles).

account, shown in Fig. 8(a). The system output power $P_{\mathrm{out,sys}}$, which is the sum $P_{\mathrm{LVdc}} + P_{\mathrm{LVac}}$ in quadrant 1, can be calculated. The average weighted system efficiency

$$\bar{\eta}_{\mathrm{sys}}(\xi) = \frac{\sum\limits_{(P_{\mathrm{LVac}}\ P_{\mathrm{LVdc}})\in M} \eta_{\mathrm{sys}}(\xi, P_{\mathrm{LVac}}, P_{\mathrm{LVdc}})\,(P_{\mathrm{LVdc}}+P_{\mathrm{LVac}})}{\sum\limits_{(P_{\mathrm{LVac}}\ P_{\mathrm{LVdc}})\in M} P_{\mathrm{LVdc}} + P_{\mathrm{LVac}}} \tag{4}$$

is used to evaluate the topology configuration influence. This calculation is done for all possible link ratios, and the link ratio with highest average weighted efficiency is considered optimal. The system efficiency is calculated as described in Section II for each operation point. The average weighted system efficiency considers the fact that the overall losses during operation are influenced by high efficiencies at high system output power $P_{\mathrm{out,sys}}$ more than having the same efficiency benefit for low system output power.

In the second approach, the categories/segments of the operational area which are displayed in Fig. 4 are used. The direct influence of the link ratio on the position of the local efficiency optimum - as shown in Section III-A - is exploited. In this approach, the weighted Center of the Mission profile trajectory (CoM) is calculated.

$$\begin{bmatrix} P_{\mathrm{LVac,CoM}} \\ P_{\mathrm{LVdc,CoM}} \end{bmatrix} = \frac{\sum\limits_{(P_{\mathrm{LVac}}\ P_{\mathrm{LVdc}})\in M} (P_{\mathrm{LVdc}} + P_{\mathrm{LVac}}) \begin{bmatrix} P_{\mathrm{LVac}} \\ P_{\mathrm{LVdc}} \end{bmatrix}}{\sum\limits_{(P_{\mathrm{LVac}}\ P_{\mathrm{LVdc}})\in M} P_{\mathrm{LVdc}} + P_{\mathrm{LVac}}} \tag{5}$$

Here, a weight by the overall output power is assigned to each operation point. The CoM is used as characterizing quantity of the mission profile trajectory. Hereby, the overall mission profile is represented by a single constant load. In the second step of this design procedure, the link ratio ξ is chosen according to the category/segment of the operational area in which the CoM is located (Fig. 8(b)). The advantage of this approach is that no calculation of the system efficiency or explicit modeling for each operation point of the trajectory is necessary.

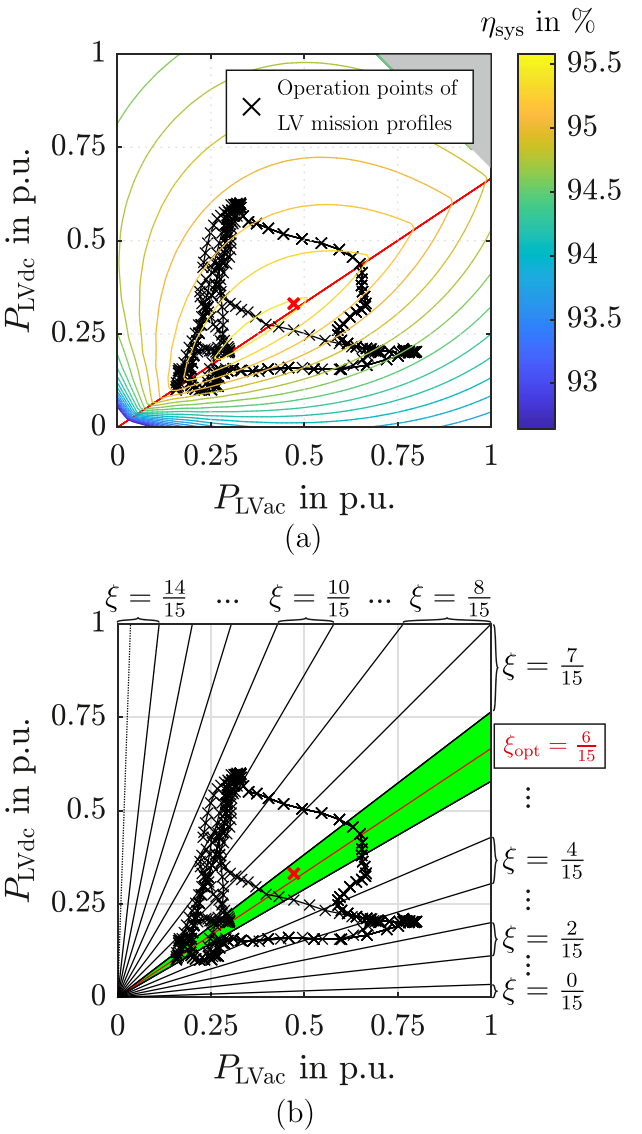

FIGURE 8. (a) System efficiency η_{sys} for constant link ratio $\xi = \frac{6}{15}$, trajectory of mission profile for LVdc use case 2 and G0; highlighted as red line: constraint (3) for unloaded interconnection DAB ($\xi_{\mathrm{opt}} = \frac{6}{15}$), highlighted as red cross: CoM. (b) Concept of CoM design approach; highlighted in green and with red line: corresponding segment and optimal link ratio $\xi_{\mathrm{opt,CoM}} = \frac{6}{15}$ from constraint (3), respectively.

IV. EFFICIENCY OPTIMIZATION FOR HYBRID GRID CONNECTING CONVERTER ARCHITECTURE

The optimization procedure is executed for quadrant 1, where active power is consumed by both LV grids. Reverse power flow from LV to supply grids comes with challenges [23], this is why quadrant 3 is excluded for this analysis. In quadrants 2 and 4 the same challenge arises in case one LV grid consumes less power than the other one provides. Furthermore, these quadrants only allow a limited opportunity for system

TABLE 1. Optimal Link Ratio of Both PRD Algorithms

$\xi_{\text{opt},\eta}$		LVac		
$\xi_{\text{opt,CoM}}$		G0	G6	H0
LVdc	Use case 1	7/15	8/15	8/15
	(High EV, high PV)	7/15	8/15	7/15
	Use case 2	6/15	7/15	7/15
	(Low EV, low PV)	6/15	7/15	6/15
	Use case 3	7/15	7/15	7/15
	(const. base load)	7/15	8/15	7/15

efficiency optimization, because the choice is only between maximum and minimum link ratio (Fig. 4).

In Fig. 8(a), the system efficiency for link ratio $\xi = \frac{6}{15}$ and the operation points trajectory for use case 2 of the LVdc profile and G0 profile are shown. The condition for an unloaded interconnecting DAB and the CoM are highlighted. An optimal link ratio $\xi_{\text{opt},\eta} = \frac{6}{15}$ is suggested by the approach of average weighted system efficiency in this case. Compared to the NIT, using the IT with the optimal link ratio can improve the average weighted system efficiency by more than 0.74 $\Delta\%$. The second approach using the category location of the CoM also indicates an optimal link ratio of $\xi_{\text{opt,CoM}} = \frac{6}{15}$.

Both approaches are compared for all combinations of load profiles, the results are shown in Table 1. Almost all combinations of LV profiles lead to the same optimal link ratio from both approaches. In case the two approaches suggest different link ratios, the difference of average system efficiency $\Delta\bar{\eta}_{\text{sys}} = \bar{\eta}_{\text{sys}}(\xi_{\text{opt},\eta}) - \bar{\eta}_{\text{sys}}(\xi_{\text{opt,CoM}})$ is examined. Due to the small variation in the average efficiency for link ratios around the optimal value, the differences in the average efficiency which stem from the different link ratios are small, less than 0.003 $\Delta\%$ (use case 3, G6), 0.022 $\Delta\%$ (use case 1, H0) and 0.008 $\Delta\%$ (use case 2, H0). Concluding, the CoM approach is the preferred choice, because a sufficiently precise design choice for the configuration can be made without the efficiency calculation and its computational burden potentially allowing for online applications based on load data forecast or measurements. For all mission profile combinations, using the IT with an optimal link ratio increases the average system efficiency between 0.65 $\Delta\%$ and 1.17 $\Delta\%$ compared to the NIT.

An adapted trajectory of operation points, e.g. by increase of EV integration in the LVdc grid, is one use case that exploits the benefits of the IT together with the PRD approach. A new optimal link ratio is chosen in case of further EV integration and the link ratio can be adapted to still achieve optimal efficiency. Furthermore, online adaption of the link ratio is possible to split the trajectory of the mission profile into several parts and realize an optimal link ratio for each of them. For changing the configuration of one MB PEBB, the PEBB has to be unloaded and removed from the normal operation of the dc-multibus converter first. Then, the output of the PEBB needs to be disconnected from the bus (dc-link or LVdc) via a mechanical switch and connected to the other bus. To avoid inrush currents during the reconnection with the other bus a precharge circuit is needed. The precharge resistor can be shorted and the PEBB loaded after the voltage of the PEBB output capacitors has balanced with the bus voltage. After the reconfiguration, the system can work in normal operation with the new optimal link ratio.

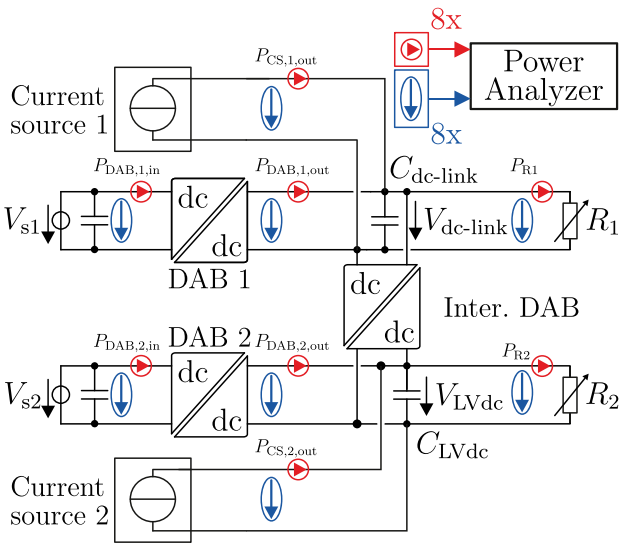

FIGURE 9. Small scale prototype of a hybrid grid connecting converter architecture with dc power supply. Voltage measurement and current measurement for efficiency calculation via power analyzer are highlighted.

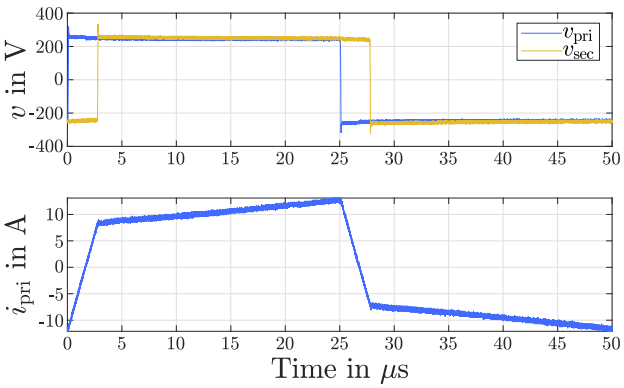

FIGURE 10. Measurements of DAB primary and secondary side voltage and primary inductor current for operation at 2 kW output power.

V. LABORATORY VALIDATION

The simulation results are validated on a small scale prototype in the laboratory. The aim is to proof the efficiency improvement by reconfigurability in dependence of loading conditions. The setup is shown in Fig. 9 and Fig. 10 shows voltage and current waveforms of DAB 1 exemplarily. An input series connected dc-multibus architecture is considered, with two MB PEBBs as DABs feeded by dc sources with voltages V_{s1} and V_{s2}. The third DAB is the interconnecting DAB, which connects the dc-link and the LVdc feeder. In comparison to the analytic analysis, the LVac converter is not

TABLE 2. Experimental Setup Parameters

Symbol	Representation	Value
V_{s1}, V_{s2}	supply side MB cell voltages	250 V
$V_{dc-link}$ / V_{LVdc}	LV dc-link / LVdc grid voltage	250 V
$C_{dc-link}$ / C_{LVdc}	dc-link / LVdc grid capacitor	4.5 mF
L_{DAB}	DAB inductances	65 µH
n	Transformer turn ratio	1
$f_{sw,DAB}$	DAB switching frequency	20 kHz

considered because it plays a subordinate role in the proof of concept in the efficiency optimization. In addition to the two DABs (superscript index *dcdc*) further MB PEBBs are represented by controlled current sources with the same power transfer characteristics as the respective DABs (superscript index *cs*), transferring the same power. In total the small scale prototype has $N_{MB} = 4$ PEBBs where the total number of PEBBs connected to the dc-link is given as $N_{MB,dc-link} = N^{cs}_{MB,dc-link} + N^{dcdc}_{MB,dc-link}$ and accordingly for the PEBBs connected to the LVdc grid $N_{MB,LVdc} = N^{cs}_{MB,LVdc} + N^{dcdc}_{MB,LVdc}$ while (1) and (3) can be used analogously. With this approach, further PEBBs can be emulated. For the current sources, power setpoints are given, for current source 1 as $P_{CS,1,out} = N^{cs}_{MB,dc-link} P_{DAB,1,out}$ and for current source 2 as $P_{CS,2,out} = N^{cs}_{MB,LVdc} P_{DAB,2,out}$ according to the total number of PEBBs and the link ratio. It is possible to adapt the configuration of the setup and connect a certain number of DABs to the dc-link or the LVdc feeder. The detailed control schemes are given in [16]. The grid loads P_{LVac} and P_{LVdc} are represented by the variable resistive loads R_1 and R_2, comprised of parallel passive and electric loads with the output powers P_{R1} and P_{R2}. In this way, the system efficiency can be calculated.

$$\eta = \frac{P_{out}}{P_{in}} = \frac{P_{R1} + P_{R2}}{P_{CS,1,in} + P_{DAB,1,in} + P_{DAB,2,in} + P_{CS,2,in}} \quad (6)$$

To consider the losses of the emulated PEBBs, the output powers $P_{CS,1,out}$ and $P_{CS,2,out}$ of the current sources need to be transferred to their input powers $P_{CS,1,in}$ and $P_{CS,2,in}$, respectively. In this manner, the additional losses are taken into account for the system efficiency calculation. For the additional PEBBs, the same efficiency characteristics as for the two DABs are assumed and the output powers are linearly scaled, leading to the equivalent input powers for the two current sources ((7) and (8)). The setup and the laboratory equipment are shown in Fig. 11. The parameters of the setup are given in Table 2.

$$P_{CS,1,in} = P_{CS,1,out} \frac{P_{DAB,1,in}}{P_{DAB,1,out}} = \frac{P_{CS,1,out}}{\eta_{DAB,1}} \quad (7)$$

$$P_{CS,2,in} = P_{CS,2,out} \frac{P_{DAB,2,in}}{P_{DAB,2,out}} = \frac{P_{CS,2,out}}{\eta_{DAB,2}} \quad (8)$$

For the validation, a total number of four cells is considered and three link ratios are evaluated for operation points highlighted in Fig. 4 with equal cumulative transferred power $P_{LVac} + P_{LVdc} = 6$ kW. The configuration parameters

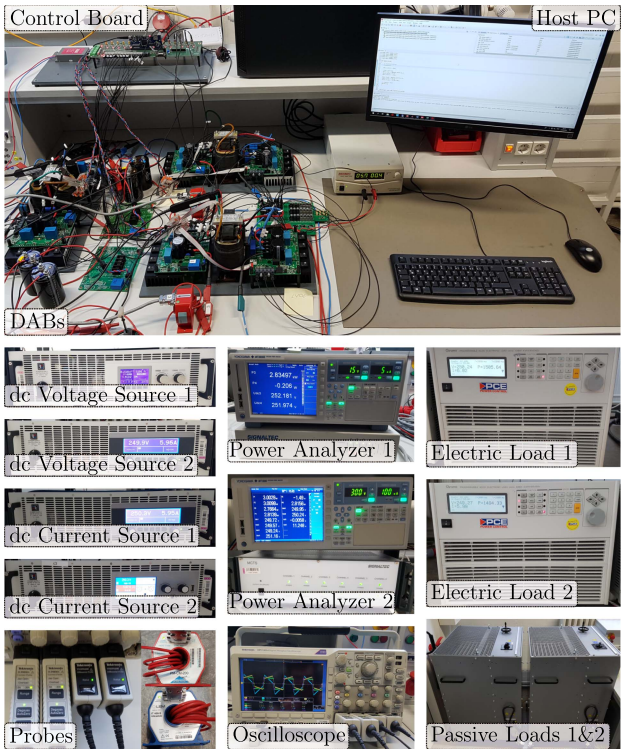

FIGURE 11. Laboratory setup and equipment used for the validation.

TABLE 3. Small Scale Prototype Configurations

ξ	N	$N^{dcdc}_{MB,dc-link}$	$N^{cs}_{MB,dc-link}$	$N^{dcdc}_{MB,LVdc}$	$N^{cs}_{MB,LVdc}$
1/4	4	1	2	1	0
2/4	4	1	1	1	1
3/4	4	1	0	1	2

are listed in Table 3. In Fig. 12 the measured system efficiency for the link ratios $\xi = \left[\frac{1}{4}, \frac{2}{4}, \frac{3}{4}\right]$ is shown. With increasing power P_{R1} a high link ratio becomes less beneficial while a small link ratio gives higher system efficiency. For a link ratio $\xi = \frac{2}{4}$ the measured system efficiency gives a symmetric behavior with respect to the equal power distribution $\frac{P_{R1}}{P_{R2}} = 1$. Like in Fig. 5, an optimal link ratio for certain operation points can be identified. Two aspects must be taken into account. Firstly, the LVac converter is not considered in the laboratory setup, because it does not influence the concept of PRD. Therefore - in contrast to the simulation results shown in Fig. 5 - the measured efficiency $\eta_{sys}\left(\frac{P_{R1}}{P_{R2}}, \xi\right)$ should be mirrored with respect to the output powers and the cell configuration, so $\eta_{sys}\left(\frac{P_{R1}}{P_{R2}}, \xi\right) = \eta_{sys}\left(\frac{P_{R2}}{P_{R1}}, 1 - \xi\right)$ should hold for all operation points. Secondly, the described symmetry is not given for the laboratory results, due to the reason that both DABs have different efficiency curves, which are shown in Fig. 13. The first DAB has a lower efficiency for all operation points, which stems from higher losses induced by manufacturing tolerances in the high-frequency transformer. This difference leads to distorted results for the system efficiency (6), because

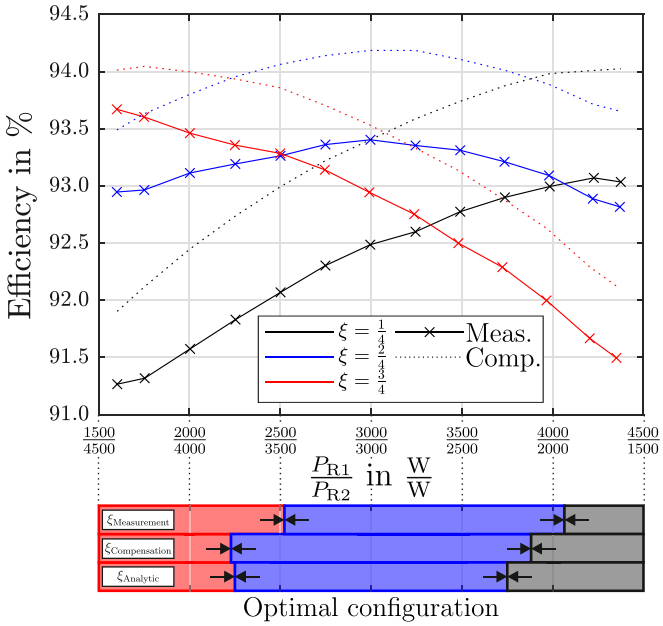

FIGURE 12. Measured (*Meas.*) system efficiency η_{sys} for different link ratios ξ with operations points highlighted in Fig. 4 with $P_{LVac} + P_{LVdc} = 6$ kW. The results for compensating (*Comp.*) the inequality of the DAB efficiencies are given as well. In addition, the optimal link ratio for different operation areas is highlighted for the measured and the compensated laboratory results and the theoretical analysis (3).

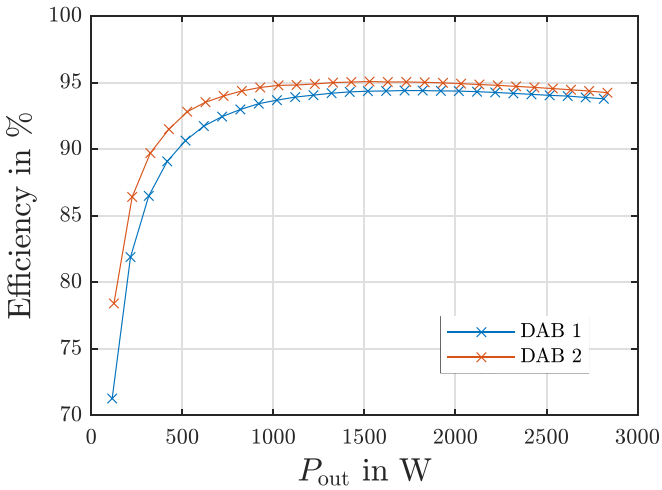

FIGURE 13. Measured efficiency curves $\eta(P_{out})$ of the two DABs in dependence of the output power P_{out}.

the individual efficiencies of the DABs take a major role in the calculation of the input power of the emulated PEBBs ((7) and (8)). Therefore, (7) is replaced by

$$P'_{CS,1,in} = \frac{P_{CS,1,out}}{\eta_{DAB,2}} \tag{9}$$

and inserted together with

$$P'_{DAB,1,in} = P_{DAB,1,out}\frac{P_{DAB,2,in}}{P_{DAB,2,out}} = \frac{P_{DAB,1,out}}{\eta_{DAB,2}} \tag{10}$$

into the efficiency calculation (6). Hereby, the efficiency of DAB 2 is assumed for all four PEBBs - and calculated from the efficiency curve in Fig. 13 - to focus on the influence of the reconfiguration and exclude the manufacturing tolerances. As can be seen in Fig. 13, the system efficiency including the compensation gives a more symmetrical behavior and leads to results close to the results from the analytic calculations. Overall, the link ratio influence on the system efficiency with the aim to choose a link ratio that gives optimal efficiency can be validated in the laboratory. A reconfiguration of cells is beneficial for the system efficiency.

VI. CONCLUSION

The possibility of power transfer from supply to LVdc grid and vice versa with a reduced number of conversion stages as well as internal passive power routing are enabled by the investigated hybrid grid connecting converter architecture in an interconnected topology. To increase the system efficiency of power transfer, the configuration of the modular multibus structure is adapted by employing *Power Routing by Design*. With the two proposed mission profile-based design approaches it is possible to find an optimal link ratio configuration. The first uses a system efficiency calculation based on analytic equations, whereas the second works with pure knowledge of the loading conditions. An absolute increase of the system efficiency by up to 3.0 % is possible for certain loading conditions and an absolute increase of the average weighted system efficiency of about 1.0 % can be realized with this efficiency optimization for the considered mission profiles. The laboratory experiments validate the potential for efficiency improvement by the optimal choice for topology reconfiguration of the modular dc-multibus.

REFERENCES

[1] M. Stecca, L. R. Elizondo, T. B. Soeiro, P. Bauer, and P. Palensky, "A comprehensive review of the integration of battery energy storage systems into distribution networks," *IEEE Open J. Ind. Electron. Soc.*, vol. 1, pp. 46–65, 2020.

[2] L. Wang, Z. Qin, T. Slangen, P. Bauer, and T. van Wijk, "Grid impact of electric vehicle fast charging stations: Trends, standards, issues and mitigation measures - an overview," *IEEE Open J. Power Electron.*, vol. 2, pp. 56–74, 2021.

[3] G. Rituraj, G. R. C. Mouli, and P. Bauer, "A comprehensive review on off-grid and hybrid charging systems for electric vehicles," *IEEE Open J. Ind. Electron. Soc.*, vol. 3, pp. 203–222, 2022.

[4] O. D. Montoya, W. Gil-Gonzalez, and A. Garces, "Optimal power flow on DC microgrids: A quadratic convex approximation," *IEEE Trans. Circuits Syst. II, Exp. Briefs*, vol. 66, no. 6, pp. 1018–1022, Jun. 2019.

[5] D. Salomonsson, L. Soder, and A. Sannino, "Protection of low-voltage DC microgrids," *IEEE Trans. Power Del.*, vol. 24, no. 3, pp. 1045–1053, Jul. 2009.

[6] T. Dragicevic, X. Lu, J. C. Vasquez, and J. M. Guerrero, "DC microgrids-part II: A review of power architectures, applications, and standardization issues," *IEEE Trans. Power Electron.*, vol. 31, no. 5, pp. 3528–3549, Jan. 2016.

[7] D. Kumar, F. Zare, and A. Ghosh, "DC microgrid technology: System architectures, AC grid interfaces, grounding schemes, power quality, communication networks, applications, and standardizations aspects," *IEEE Access*, vol. 5, pp. 12230–12256, 2017.

[8] X. Liu, P. Wang, and P. C. Loh, "A hybrid AC/DC microgrid and its coordination control," *IEEE Trans. Smart Grid*, vol. 2, no. 2, pp. 278–286, Mar. 2011.

[9] F. Nejabatkhah and Y. W. Li, "Overview of power management strategies of hybrid AC/DC microgrid," *IEEE Trans. Power Electron.*, vol. 30, no. 12, pp. 7072–7089, Dec. 2015.
[10] N. Eghtedarpour and E. Farjah, "Power control and management in a hybrid AC/DC microgrid," *IEEE Trans. Smart Grid*, vol. 5, no. 3, pp. 1494–1505, May 2014.
[11] M. Pavlovsky, G. Guidi, and A. Kawamura, "Assessment of coupled and independent phase designs of interleaved multiphase buck boost DC–DC converter for EV power train," *IEEE Trans. Power Electron.*, vol. 29, no. 6, pp. 2693–2704, Jun. 2014.
[12] M. Rolak, C. Sobol, M. Malinowski, and S. Stynski, "Efficiency optimization of two dual active bridge converters operating in parallel," *IEEE Trans. Power Electron.*, vol. 35, no. 6, pp. 6523–6532, Jun. 2020.
[13] S. Madhusoodhanan et al., "Solid-state transformer and MV grid tie applications enabled by 15 kV SiC IGBTs and 10 kV SiC MOSFETs based multilevel converters," *IEEE Trans. Ind. Appl.*, vol. 51, no. 4, pp. 3343–3360, Jul./Aug. 2015.
[14] D. Dujic et al., "Power electronic traction transformer-low voltage prototype," *IEEE Trans. Power Electron.*, vol. 28, no. 12, pp. 5522–5534, Dec. 2013.
[15] J. Schaumburg, J. Kuprat, M. Langwasser, and M. Liserre, "Efficiency optimization via mission profile-based design of a hybrid grids-feeding smart transformer," in *Proc. IEEE 13th Int. Symp. Power Electron. Distrib. Gener. Syst.*, 2022, pp. 1–6.
[16] J. Kuprat, J. Schaumburg, M. Langwasser, and M. Liserre, "Mission-profile based design of a hybrid-grids feeding smart transformer," in *Proc. 6th IEEE Workshop Electron. Grid*, 2021, pp. 01–08.
[17] W. Liu, J. Liao, Y. Hong, L. Huang, X. Hao, and X. Lei, "Control strategy of energy routers for AC/DC hybrid distribution network with closed loop operation in short time scale," in *Proc. 5th Int. Conf. Power Renewable Energy*, 2020, pp. 366–371.
[18] J. Khodabakhsh and G. Moschopoulos, "Uncertainty reduction for data centers in energy internet by a compact AC–DC energy router and coordinated energy management strategy," in *Proc. IEEE Energy Convers. Congr. Expo.*, 2020, pp. 4668–4673.
[19] J. Kuprat, M. Andresen, V. Raveendran, and M. Liserre, "Modular smart transformer topology for the interconnection of multiple isolated AC and DC grids," in *Proc. IEEE Energy Convers. Congr. Expo.*, 2020, pp. 4836–4841.
[20] J. Kuprat, J. Schaumburg, M. Langwasser, and M. Liserre, "Improved graph-theory based modeling of the smart transformer for hybrid grids," in *Proc. IEEE 16th Int. Conf. Compat., Power Electron., Power Eng.*, 2022, pp. 1–6.
[21] H. Vermeulen and T. Nieuwoudt, "Optimisation of residential solar PV system rating for minimum payback time using half-hourly profiling," in *Proc. Int. Conf. Domestic Use Energy*, 2015, pp. 215–221.
[22] P. Djapic et al., "Design and real-time control of smart distribution networks," Low Carbon London, Imperial College London, London, Tech. Rep. D3, 2014.
[23] G. De Carne, G. Buticchi, Z. Zou, and M. Liserre, "Reverse power flow control in a ST-Fed distribution grid," *IEEE Trans. Smart Grid*, vol. 9, no. 4, pp. 3811–3819, Jul. 2018.

JOSCHA SCHAUMBURG received the B.Sc. degree in power engineering from Leibniz University Hanover, Hanover, Germany, in 2017, and the M.Sc. degree in electrical engineering from Kiel University, Kiel, Germany, in 2020. He is currently working toward the Ph.D. degree with the Chair of Power Electronics, Kiel University, focusing on smart transformer for hybrid grids and reliability of power electronics systems. His research interests include smart transformers, hybrid grids, multi-objective power routing, reliability in power electronics, real-time simulation, and modeling of converters in power-hardware-in-the-loop environments.

JOHANNES KUPRAT (Graduate Student Member, IEEE) received the M.Sc. degree in electrical engineering and business administration from Kiel University, Kiel, Germany, in 2019. Afterwards, he started the Ph.D. degree with the Chair of power electronics, Kiel University focusing on the reliability of the smart transformer and its application for hybrid grids. His research interests include smart transformers, reliability in power electronics, hybrid grids, active thermal control, multi-objective power routing, junction temperature sensing and estimation, and digital twins.

MARIUS LANGWASSER (Member, IEEE) received the M.Sc. and Ph.D. degrees from Kiel University, Kiel, Germany, in 2016 and 2021, respectively. He is currently a Senior Postdoctoral Scientific Staff Member and the Leader of the Group "Hybrid Grids," Chair of Power Electronics, Kiel University. He is responsible for the Kopernikus-Project ENSURE and Marie Sklodowska-Curie Research Actions Wingrid and SMARTGYsum. His research interests include control and protection of meshed and hybrid grids, dynamically reconfigurable grids and grid service provision with high-voltage direct current (HVdc) systems and smart transformers.

MARCO LISERRE (Fellow, IEEE) received the M.Sc. and Ph.D. degrees in electrical engineering from the Polytechnic University of Bari, Bari, Italy, in 1998 and 2002, respectively. He has been an Associate Professor with the Polytechnic University of Bari, Bari, Italy. Since 2012, he has been a Professor of reliable power electronics with Aalborg University, Aalborg, Denmark. Since 2013, he has been a Full Professor and holds the Chair of power Eeectronics with Kiel University, Kiel, Germany. He got offered and declined professorships with the Technical University of Ilmenau, Ilmenau, Germany, Technical University of Munich, Munich, Germany, and Technical University of Hamburg, Hamburg, Germany. In 2022, he joined, part-time, Fraunhofer ISIT, Itzehoe, Germany, as the Deputy Director and the Director of a new Center for Electronic Energy Systems funded for five million Euros. He has authored or coauthored more than 600 technical papers (1/3 of them in international peer-reviewed journals), a book, and two granted patents, with more under evaluation, some of them involving companies. These works have received more than 45 000 citations. He was listed in ISI Thomson Report "The Worlds Most Influential Scientific Minds" in 2014.

Dr. Liserre is also a Member of the IEEE Industry Applications Society (IAS), IEEE Power Electronics Society (PELS), IEEE Power and Energy Society (PES), and IEEE Industrial Electronics Society (IES), and has been serving all these societies in different capacities. He was the recipient of the IES 2009 Early Career Award, IES 2011 Anthony J. Hornfeck Service Award, 2014 Dr. Bimal Bose Energy Systems Award, 2017 IEEE PELS Sustainable Energy Systems Technical Achievement Award, 2018 IEEE IES Mittelmann Achievement Award, and six IEEE Journal Awards. In PELS, he is an AdCom Member (second mandate), the Co-Editor of the IEEE Open Journal of Power Electronics, an Associate Editor for the IEEE Transactions on Power Electronics and IEEE Journal of Emerging and Selected Topics in Power Electronics (JESTPE), the Guest Editor of several special issues of JESTPE, the Technical Committee Chairperson of the new Committee on Electronic Power Grid Systems, a Member of the IEEE Digital Committee, IES Liaison responsible, eGrid 2021 Workshop Co-Chairperson, and PEDG 2022 Co-Chairperson.